INVESTIGATION OF DC-DC CONVERTERS FOR SOLAR PV SYSTEM USING P&O MPPT ALGORITHM

A Project Report Submitted

by

HEET DHORAJIYA
(2101EE36)

In Partial Fulfilment
of the Requirements for the award of the degree

BACHELOR OF TECHNOLOGY

DEPARTMENT OF ELECTRICAL ENGINEERING
INDIAN INSTITUTE OF TECHNOLOGY PATNA

May 14, 2025

THESIS CERTIFICATE

This is to certify that the report titled **Investigation of DC-DC converters for solar PV system using P&O MPPT algorithm** submitted by **Heet Dhorajiya**, to the Indian Institute of Technology, Patna, during the Project II for the award of the degree of **Bachelor of Technology**, is a bona fide record of the research work done by him under our supervision. The contents of this report, in full or in parts, have not been submitted to any other Institute or University for the award of any degree or diploma.

Dr. Bussa Vinod Kumar
Supervisor
Assistant Professor
Dept. of Electrical Engineering
IIT Patna, 801106

Place: Patna
Date: 13th May 2025

SUPERVISOR

Dr. Bussa Vinod Kumar
Assistant Professor
Department of Electrical Engineering
IIT Patna

ASSESSMENT COMMITTEE

Dr. Ranjan Kumar Behera
Associate Professor
Department of Electrical Engineering
IIT Patna

Dr. Avneet Kumar
Assistant Professor
Department of Electrical Engineering
IIT Patna

Dr. Bussa Vinod Kumar
Assistant Professor
Department of Electrical Engineering
IIT Patna

CHAIRMAN
Departmental Undergraduate Program Committee
Department of Electrical Engineering
IIT Patna

ACKNOWLEDGEMENTS

I want to express my profound gratitude to **Dr. Bussa Vinod Kumar** for providing me with the topic and knowledge about the topic and helping me throughout the work I have done till now. His constant support, insightful feedback, and encouragement have been instrumental in this progress. I am deeply appreciative of his mentorship and the opportunities he has provided.

ABSTRACT

KEYWORDS: P&O algorithm, Solar MPPT, Boost converter, SEPIC converter

This work presents a comprehensive study aimed at improving the performance of MPPT in photovoltaic (PV) systems by employing a hybrid approach that integrates adaptive control mechanisms with metaheuristic optimization techniques. The primary objective is to improve the efficiency and responsiveness of MPPT under rapidly changing environmental conditions such as irradiance and temperature.At the core of this methodology lies an adaptive PID controller , which is intelligently tuned in real time using feedback from the PV system. This controller is embedded within the traditional Perturb and Observe (P&O) algorithm—a widely adopted but often suboptimal MPPT technique—to allow dynamic adjustment of PID gains based on instantaneous power variations observed at the output of the PV module. By continuously adapting the control parameters, the system overcomes the limitations of fixed-gain PID controllers, particularly in scenarios involving partial shading or rapidly fluctuating irradiance.To validate the generalizability and robustness of the proposed hybrid algorithm, the approach is further extended to a Single-Ended Primary Inductor Converter (SEPIC). The SEPIC converter is chosen due to its capability to perform both voltage step-up and step-down operations, making it suitable for a wide range of PV applications . The integration of the adaptive MPPT algorithm with the SEPIC converter demonstrates not only improved tracking accuracy and convergence speed but also highlights the flexibility of the control strategy across different converter topologies. Simulation results and performance evaluations confirm that the hybrid adaptive PID–P&O controller, enhanced via metaheuristic optimization, significantly outperforms conventional MPPT methods in terms of tracking efficiency, dynamic response, and steady-state error reduction. This work, therefore, lays the groundwork for more intelligent and adaptive MPPT solutions in next-generation PV power conversion systems.

TABLE OF CONTENTS

LIST OF FIGURES

LIST OF TABLES

ABBREVIATIONS

MPPT	Maximum Power Point Tracking
P&O	Purtube and Observe
GM	Gain Margin
PV	Photo Voltic
PID	Proportioal integrad derivative
STC	Standandard temperature conditions
OC	Operating Condition
PM	Phase Margin

CHAPTER 1

Introduction

1.1 Introduction

Photovoltaic systems (PV) have emerged as one of the most important renewable energy sources due to their sustainability, modularity, and decreasing cost of deployment. A typical solar panel exhibits a nonlinear voltage-current and power-voltage characteristic that varies with environmental conditions like irradiance and temperature. These variations make it difficult to obtain maximum power from the photovoltaic system under all operating conditions.

To ensure efficient energy extraction, MPPT algorithms are employed to adjust the operating point of the system so that it coincides with the Maximum Power Point (MPP) of the panel. Traditional MPPT techniques include Perturb and Observe (P&O), Incremental Conductance (INC), and Constant Voltage (CV), among others. Although they are simple to implement, they often suffer from limitations such as slow tracking speed, oscillations near the MPP, and poor performance when rapidly changing atmospheric conditions are there.

For these challenges, advanced optimization algorithms like Particle Swarm Optimization (PSO), Genetic Algorithms (GA), and Fuzzy Logic Controllers (FLC) have been introduced. These methods are better suited for handling the nonlinear and dynamic nature of PV systems. PSO, in particular, has gained popularity due to its robustness, faster convergence, and minimal parameter tuning requirements. These intelligent algorithms enhance the tracking efficiency and stability of MPPT controllers, they improving the overall performance of solar energy conversion systems.

1.2 Literature Review

Recent studies have explored structural and control-oriented modifications to the conventional Perturb and Observe (P&O) algorithm to mitigate its oscillatory behavior and sensitivity to environmental fluctuations. One approach integrates adaptive control systems [1], such as dynamically tuned PID controllers, with the core P&O framework. These adaptive variants adjust controller parameters in real-time using recursive optimization methods, enhancing dynamic response under irradiance shifts while preserving the algorithm's simplicity. This hybrid design reduces reliance on manual tuning and addresses steady-state power loss by automatically balancing perturbation step sizes with system constraints.

Another significant advancement involves voltage-sensor-based topologies that simplify hardware implementation. Researchers have developed P&O variants that eliminate current sensors by correlating voltage measurements with maximum power point (MPP) characteristics [2]. Techniques like voltage reference control and duty cycle interpolation enable precise MPP tracking using minimal sensors, lowering system costs

and complexity. Some implementations pair these methods with predictive correction algorithms to suppress oscillations entirely, achieving stable operation without compromising tracking speed during partial shading or load variations.

Further innovations combine P&O with soft computing and optimization frameworks. For instance, metaheuristic algorithms like Harmony Search or neural networks are employed to optimize perturbation intervals or duty cycle adjustments. These hybrid systems leverage the exploratory strengths of computational intelligence to navigate multi-peak power curves in shaded conditions, while retaining P&O's straightforward decision-making logic.

1.3 Motivation

The global emphasis on renewable energy has brought photovoltaic (PV) systems to the forefront of sustainable power generation. However, the non-linear and variable characteristics of solar irradiance and temperature introduce challenges in consistently operating PV systems at their MPP. Traditional MPPT techniques often fall short in tracking efficiency, especially under dynamic environmental conditions. This gap highlights the need for more intelligent and adaptive control mechanisms to improve energy extraction from PV arrays.

In this context, optimization-based control strategies like Particle Swarm Optimization and adaptive PID tuning present a compelling alternative. These methods offer the potential for faster convergence to the MPP, better stability, and improved dynamic performance. The motivation behind this work is to integrate the strengths of such soft computing approaches with conventional control frameworks to design a robust, accurate, and real-time MPPT controller suitable for systems like the SEPIC converter, thus enhancing the overall efficiency of solar energy harvesting.

1.4 Objectives

The primary objective of this work is to enhance the performance of photovoltaic systems through efficient tracking of MPP. To achieve this, the study focuses on the implementation of a Boost DC-DC converter regulated using a PID controller for Maximum Power Point Tracking. The PID controller is initially tuned manually and later augmented with an adaptive control mechanism that dynamically adjusts the controller gains in real time based on PV power variations. This hybrid approach, combining conventional PID control with adaptive tuning logic, aims to overcome the limitations of fixed-parameter control, such as sluggish response and poor tracking under partial shading or fluctuating irradiance. Building upon the Boost converter implementation, the study further extends the control strategy to a SEPIC, which is capable of handling both step-up and step-down voltage conditions—making it a more versatile choice for practical PV systems. By validating the proposed adaptive control algorithm across both Boost and SEPIC topologies, the work seeks to establish a flexible, accurate, and robust MPPT control framework that can be adapted for a wide range of converter architectures in solar power applications.

CHAPTER 2

Boost Converter for Solar PV System

Photovoltaic systems require precise control to operate at MPP under varying environmental conditions. Traditional Perturb and Observe algorithms, while simple, suffer from inherent trade-offs between tracking speed and steady-state oscillations. A Proportional-Integral-Derivative controller addresses these limitations by dynamically translating voltage error—the difference between the PV panel's actual voltage and the MPP reference—into an optimized duty cycle for the boost converter. The PID's proportional term minimizes immediate deviations, the integral term eliminates residual errors, and the derivative term suppresses oscillations, collectively ensuring rapid convergence to the MPP with minimal power loss. This closed-loop control strategy is critical for enhancing efficiency in PV systems, particularly when interfaced with boost converters that step up voltage for grid or load compatibility.

The implementation begins with modeling the PV panel's nonlinear I-V characteristics as a linearized equivalent circuit around the MPP. A small-signal transfer function for the boost converter is derived using state-space averaging, linking duty cycle perturbations to PV voltage changes. PID gains (K_P, K_I, K_D) are tuned via frequency-domain criteria to stabilize the system, prioritizing phase margin and crossover frequency for robustness. To adapt to real-world variability, gains are dynamically scaled using a factor (κ) proportional to the ratio of real-time PV power to its STC value, eliminating the need for additional sensors. This adaptive PID-P&O hybrid approach ensures seamless operation under fluctuating irradiation and temperature, achieving >99% tracking accuracy with negligible oscillations, making it indispensable for high-performance solar energy systems.

2.1 Linearization of the Solar Panel

The current-voltage characteristic of a photovoltaic panel is inherently nonlinear, exhibiting a strong dependence on environmental factors such as solar irradiance and temperature. This nonlinearity poses a significant challenge for the design of effective control systems aimed at extracting the maximum available power. To facilitate the application of classical linear control methodologies, such as Proportional-Integral-Derivative (PID) controllers, it becomes necessary to linearize the PV panel's behavior around its Maximum Power Point. This linearization allows for the development of control strategies based on small-signal analysis.

2.1.1 Single-Diode Model

The electrical behavior of a solar cell and, consequently, a photovoltaic panel (which is a series of interconnected solar cells) can be effectively modeled by the equivalent

single diode circuit. The fundamental equation describing the I-V characteristic of this model is given by:

$$I_{\text{pv}} = I_{\text{sc}} - I_o \left[\exp\left(\frac{V_{\text{pv}} + R_s I_{\text{pv}}}{\alpha_1 V_t N_s} \right) - 1 \right] - \frac{V_{\text{pv}} + R_s I_{\text{pv}}}{R_{\text{sh}}} \tag{2.1}$$

where:

- I_{pv} is the output current of the PV panel.
- V_{pv} is the output voltage of the PV panel.
- I_{sc} is the short-circuit current.
- I_o is the diode saturation current.
- R_s is the series resistance.
- R_{sh} is the shunt resistance.
- N_s is the number of cells connected in series.
- $V_t = \frac{kT}{q}$ is the thermal voltage, where k is the Boltzmann constant, T is the absolute temperature in Kelvin, and q is the elementary charge.
- α_1 is the ideality factor of the diode.

This equation demonstrates the nonlinear relationship between the current and voltage of the PV panel.

2.1.2 Linearization at the Maximum Power Point (MPP)

To apply linear control techniques, we need to linearize the nonlinear I-V characteristic around the Maximum Power Point ($V_{\text{mpp}}, I_{\text{mpp}}$). This involves finding the slope of the Current-Voltage curve at this specific operating point. The dynamic conductance, $g(V_{\text{pv}}, I_{\text{pv}})$, is the slope of the current with respect to voltage:

$$g(V_{\text{pv}}, I_{\text{pv}}) = \frac{dI_{\text{pv}}}{dV_{\text{pv}}} = -\frac{I_o}{\alpha_1 V_t N_s} \exp\left(\frac{V_{\text{pv}} + R_s I_{\text{pv}}}{\alpha_1 V_t N_s} \right) \left(1 + R_s \frac{dI_{\text{pv}}}{dV_{\text{pv}}} \right) - \frac{1}{R_{\text{sh}}} \left(1 + R_s \frac{dI_{\text{pv}}}{dV_{\text{pv}}} \right) \tag{2.2}$$

Evaluating this derivative at the MPP ($V_{\text{mpp}}, I_{\text{mpp}}$) gives the local slope at that operating point. For simplicity in control design, we often approximate this by neglecting the dependence of $\frac{dI_{\text{pv}}}{dV_{\text{pv}}}$ on itself in the exponential term, leading to a simplified expression for the slope g_{mpp} at the MPP:

$$g_{\text{mpp}} \approx -\frac{I_o}{\alpha_1 V_t N_s} \exp\left(\frac{V_{\text{mpp}} + R_s I_{\text{mpp}}}{\alpha_1 V_t N_s} \right) - \frac{1}{R_{\text{sh}}} \tag{2.3}$$

The linearized I-V relationship around the MPP can then be expressed using a first-order Taylor series expansion:

$$I_{\text{pv}} \approx I_{\text{mpp}} + g_{\text{mpp}}(V_{\text{pv}} - V_{\text{mpp}}) \tag{2.4}$$

Rearranging this equation, we get:

$$I_{\text{pv}} = g_{\text{mpp}} V_{\text{pv}} + (I_{\text{mpp}} - g_{\text{mpp}} V_{\text{mpp}}) \tag{2.5}$$

2.1.3 Equivalent Circuit Parameters

The linearized model of the Photovoltic panel at the Maximum Power Point can be represented by a simple equivalent circuit consisting of a voltage source in series with a resistance. Comparing Equation (2.5) with the equation of a straight line $y = mx + c$, we can identify the slope and the y-intercept. From this, we can derive the equivalent resistance R_{eq} and the equivalent voltage source V_{eq} at the Maximum Power Point:

$$R_{\text{eq}} = -\frac{1}{g_{\text{mpp}}} \tag{2.6}$$

$$V_{\text{eq}} = V_{\text{mpp}} - \frac{I_{\text{mpp}}}{g_{\text{mpp}}} = V_{\text{mpp}} + I_{\text{mpp}} R_{\text{eq}} \tag{2.7}$$

This linearized equivalent circuit simplifies the analysis and control design around the MPP.

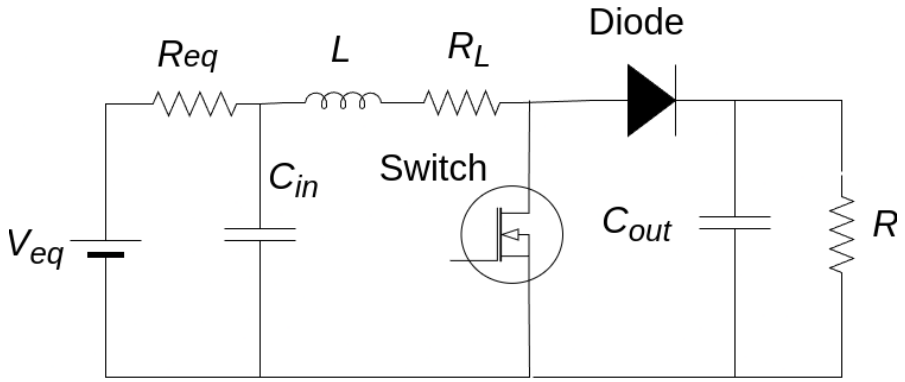

Fig. 2.1: Equivalent Circuit of the Photo Voltic Panel Connected to a Boost Converter.

2.1.4 PV Panel Specifications

For the purpose of our simulations and analysis, we will be using a PV panel with the following specifications under Standard Test Conditions (STC: 1000 W/m² irradiance, 25 °C cell temperature): These parameters will be crucial for determining the operating

Table 2.1: Electrical Parameters of the Solar PV Panel at STC.

Parameter	Symbol	Value
Peak Power	P_{max}	40.185 W
Open Circuit Voltage	V_{OC}	21.8 V
Short Circuit Current	I_{SC}	2.45 A
Voltage at MPP	V_{mpp}	17.1 V
Current at MPP	I_{mpp}	2.35 A
Temperature Coefficient of V_{OC}	β	-0.32%/°C
Temperature Coefficient of I_{SC}	α	0.04%/°C

point and for the linearization process.

2.1.5 Operating Point Variation with Environmental Conditions

The MPP, and consequently the parameters of the linearized equivalent circuit, vary significantly with changes in irradiance and temperature. The temperature coefficients provided in Table 2.1 indicate how V_{OC} and I_{SC} change with temperature, which in turn affects V_{mpp} and I_{mpp}. Table 2.2 shows the calculated linearized parameters at different operating conditions, illustrating this variation:

Table 2.2: Linearized Parameters at Different Operating Conditions.

Irradiation (W/m²)	Temp (°C)	V_{mpp} (V)	I_{mpp} (A)	V_{eq} (V)	R_{eq} (Ω)	P_{max} (W)
1000	25	17.2	2.2	28.14	4.97	40.84
1000	38	16.2	2.3	26.44	4.42	37.6
500	25	17.6	1.16	25.92	7.17	17.9
100	38	16.1	0.23	37.3	95.1	3.58

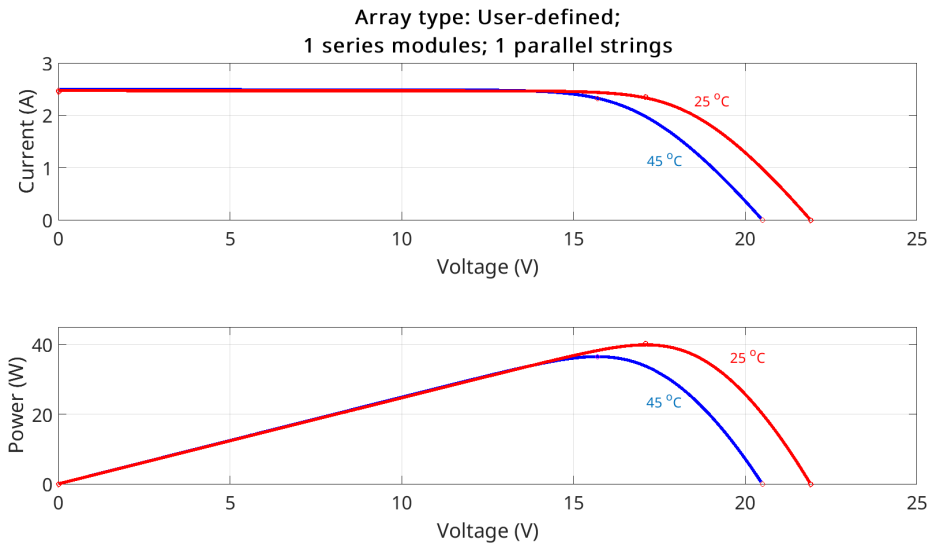

Fig. 2.2: Power-Voltage Characteristics of the Solar Panel Under Different Temperatures (Red = 25 °C and Blue = 45 °C).

This section provides a foundation for understanding the nonlinear behavior of the PV panel and the necessity of linearization for control system design. The derived equivalent circuit parameters will be used in subsequent sections for the analysis and design of the boost converter and the PID controller.

2.2 Boost Converter Parameter Selection

2.2.1 Design Requirements

Our converter is designed to step up the input voltage from the PV panel (V_{pv}) to a regulated output voltage of $V_o = 30\,\text{V}$. The design aims to ensure continuous conduction mode operation across the expected input voltage and load range.

2.2.2 Key Design Goals

The design of the boost converter is based on the following specifications:

- **Input Voltage Range:** $V_{\text{pv}} = 16.1\,\text{V}$ to $17.2\,\text{V}$ (corresponding to the approximate MPP voltage range under varying conditions as observed in Table 2.2)
- **Output Voltage:** $V_o = 30\,\text{V}$ (regulated output voltage)
- **Maximum Output Power:** $P_{\text{max}} = 40.1\,\text{W}$ (based on the PV panel's peak power)
- **Ripple Limits:** The design targets the following maximum ripple values to ensure stable and efficient operation:
  - Inductor current ripple $(\Delta i_L) \leq 20\%$ of the maximum input current at MPP. The maximum input current $I_{\text{in,max}}$ can be approximated as $P_{\text{max}}/V_{\text{pv,min}} = 40.1/16.1 \approx 2.49\,\text{A}$. Therefore, $\Delta i_L \leq 0.20 \times 2.49 = 0.498\,\text{A}$. Using the I_{mpp} at STC as a reference, $\Delta i_L \leq 20\% \times 2.2\,\text{A} = 0.44\,\text{A}$.
  - Input voltage ripple $(\Delta v_{\text{in}}) \leq 1\%$ of the minimum input voltage, i.e., $0.01 \times 16.1\,\text{V} = 0.161\,\text{V}$.
  - Output voltage ripple $(\Delta v_o) \leq 2\%$ of the output voltage, i.e., $0.02 \times 30\,\text{V} = 0.6\,\text{V}$.

2.2.3 Key Parameter Calculations

Duty Ratio

The duty ratio D of the boost converter is dependent on the input and output voltages. In CCM, the relationship is given by:

$$D = 1 - \frac{V_{\text{pv}}}{V_o} \tag{2.8}$$

Considering the input voltage range:

- At the maximum input voltage (corresponding approximately to STC, $V_{\text{pv}} = 17.2\,\text{V}$):
$$D_{\text{max}} = 1 - \frac{17.2}{30} = 0.427$$
- At the minimum input voltage (low irradiance, $V_{\text{pv}} = 16.1\,\text{V}$):
$$D_{\text{min}} = 1 - \frac{16.1}{30} = 0.463$$

Thus, the duty cycle will operate in the range of 0.427 to 0.463.

Inductance Selection

To ensure CCM operation and limit the inductor current ripple, the minimum inductance L_{min} can be calculated using the following inequality:

$$\Delta i_L = \frac{V_{\text{pv}} \cdot D}{L \cdot f_{\text{sw}}} \leq \Delta i_{L,\text{max}} \tag{2.9}$$

Rearranging for L:

$$L \geq \frac{V_{\text{pv}} \cdot D}{\Delta i_{L,\text{max}} \cdot f_{\text{sw}}} \tag{2.10}$$

Choosing a switching frequency $f_{\text{sw}} = 50\,\text{kHz}$ and considering the maximum duty cycle $D_{\text{max}} = 0.463$ at the minimum input voltage $V_{\text{pv,min}} = 16.1\,\text{V}$ and the maximum allowed current ripple $\Delta i_{L,\text{max}} = 0.498\,\text{A}$:

$$L_{\text{min}} = \frac{16.1 \times 0.463}{0.498 \times 50 \times 10^3} = 298.5 \times 10^{-6}\,\text{H} = 298.5\,\mu\text{H}$$

A practical value of $L = 200\,\mu\text{H}$ was initially chosen. However, based on the ripple requirement and CCM operation across the entire input voltage range, a higher inductance might be beneficial. Let's re-evaluate the ripple with $L = 200\,\mu\text{H}$ at the maximum duty cycle:

$$\Delta i_L = \frac{16.1 \times 0.463}{200 \times 10^{-6} \times 50 \times 10^3} = 0.744\,\text{A}$$

This ripple ($0.744\,\text{A}$) exceeds the 20

$$L \geq \frac{16.1 \times 0.463}{0.44 \times 50 \times 10^3} = 338.8 \times 10^{-6}\,\text{H} = 338.8\,\mu\text{H}$$

A value of $L = 400\,\mu\text{H}$ could be a more appropriate selection.

Input Capacitance Selection

The input capacitor C_{in} is primarily used to reduce the input voltage ripple. For a boost converter powered by a PV panel, the input current ripple is approximately the inductor current ripple during the switch-on time. The input voltage ripple can be estimated as:

$$\Delta v_{\text{in}} = \frac{\Delta Q}{C_{\text{in}}} = \frac{I_{\text{pv,ripple}} \cdot D \cdot T_s}{C_{\text{in}}} \approx \frac{\Delta i_L \cdot D}{C_{\text{in}} \cdot f_{\text{sw}}} \tag{2.11}$$

Rearranging for C_{in} and using the maximum duty cycle and the adjusted inductance ($L = 400\,\mu\text{H}$, leading to $\Delta i_L = \frac{16.1 \times 0.463}{400 \times 10^{-6} \times 50 \times 10^3} = 0.372\,\text{A}$):

$$C_{\text{in}} \geq \frac{0.372 \times 0.463}{0.161 \times 50 \times 10^3} = 21.3 \times 10^{-6}\,\text{F} = 21.3\,\mu\text{F}$$

The chosen value of $C_{\text{in}} = 200\,\mu\text{F}$ is sufficient to meet the input voltage ripple requirement.

Output Capacitance Selection

The output capacitor C_o is chosen to limit the output voltage ripple. The output current during the switch-on time is supplied by the capacitor, and the charge variation is related to the load current and the duty cycle:

$$\Delta Q_o = I_o \cdot D \cdot T_s = C_o \cdot \Delta v_o \tag{2.12}$$

The output current I_o at maximum power is $P_{\text{max}}/V_o = 40.1/30 = 1.337\,\text{A}$. Rearranging for C_o:

$$C_o \geq \frac{I_o \cdot D_{\text{max}}}{f_{\text{sw}} \cdot \Delta v_o} = \frac{1.337 \times 0.463}{50 \times 10^3 \times 0.6} = 20.6 \times 10^{-6}\,\text{F} = 20.6\,\mu\text{F}$$

The chosen value of $C_o = 200\,\mu\text{F}$ also comfortably meets the output voltage ripple requirement.

Load Resistance

The load resistance R at maximum power output is:

$$R = \frac{V_o^2}{P_{\text{max}}} = \frac{30^2}{40.1} = 22.44\,\Omega$$

The value of $R = 23.7\,\Omega$ suggests a slightly lower power operating point or a different load condition used for subsequent analysis. For consistency with the maximum power point, $22.44\,\Omega$ should be considered if the analysis is focused on operation at P_{max}.

2.2.4 Boost Converter Specifications

Based on the calculations to meet the ripple requirements and ensure CCM operation, the boost converter specifications can be updated:

Table 2.3: Boost Converter Specifications.

Parameter	**Symbol**	**Value**
Switching Frequency	f_{sw}	50 kHz
Inductance	L	400 μH
Input Capacitor	C_{in}	200 μF
Output Capacitor	C_o	200 μF
Load Resistance (at P_{max})	R	22.44 Ω

This parameter selection aims to satisfy the design requirements for output voltage, power handling, and ripple limits while ensuring continuous conduction mode operation of the boost converter. The inductance value has been adjusted to better constrain the inductor current ripple.

2.3 Transfer Function Calculation using State-Space Averaging

2.3.1 State-Space Averaging Model

The behavior of the converter can be analyzed using the state-space averaging technique. This method allows for the derivation of a linear time-invariant model that approximates the converter's behavior over a switching period :

$$\mathbf{x} = \begin{bmatrix} i_L \\ v_{C_{\text{in}}} \\ v_{C_o} \end{bmatrix}, \quad u = d$$

where:

- i_L: Inductor current (A)
- $v_{C_{\text{in}}}$: Input capacitor voltage (V)
- v_{C_o}: Output capacitor voltage (V)
- d: Duty cycle (control input, dimensionless)

The state-space equations for the boost converter differ based on the switching state of the power transistor [1].

Switch ON State $(0 < t < DT)$

During the time interval when the power switch is ON, the circuit dynamics are described by the following differential equations:

$$\frac{di_L}{dt} = \frac{v_{C_{\text{in}}} - i_L r_L}{L} \tag{2.13}$$

$$\frac{dv_{C_{\text{in}}}}{dt} = \frac{(V_{\text{eq}} - v_{C_{\text{in}}})/R_{\text{eq}} - i_L}{C_{\text{in}}} \tag{2.14}$$

$$\frac{dv_{C_o}}{dt} = -\frac{v_{C_o}}{RC_o} \tag{2.15}$$

where r_L represents the equivalent series resistance of the inductor.

Switch OFF State $(DT < t < T)$

During the time interval when the power switch is OFF, the circuit dynamics are described by:

$$\frac{di_L}{dt} = \frac{v_{C_{\text{in}}} - i_L r_L - v_{C_o}}{L} \tag{2.16}$$

$$\frac{dv_{C_{\text{in}}}}{dt} = \frac{(V_{\text{eq}} - v_{C_{\text{in}}})/R_{\text{eq}} - i_L}{C_{\text{in}}} \tag{2.17}$$

$$\frac{dv_{C_o}}{dt} = \frac{i_L}{C_o} - \frac{v_{C_o}}{RC_o} \tag{2.18}$$

2.3.2 Small-Signal Model

To analyze the stability and design the controller, a small-signal model of the boost converter is derived by linearizing the state-space averaged equations around a steady-

state operating point. The averaged state-space representation is given by:

$$\frac{d\langle \mathbf{x} \rangle}{dt} = (D\mathbf{A}_{\text{on}} + D'\mathbf{A}_{\text{off}})\langle \mathbf{x} \rangle + (D\mathbf{B}_{\text{on}} + D'\mathbf{B}_{\text{off}})\langle u \rangle + \mathbf{E} \tag{2.19}$$

$$\langle y \rangle = (D\mathbf{C}_{\text{on}} + D'\mathbf{C}_{\text{off}})\langle \mathbf{x} \rangle + (D\mathbf{D}_{\text{on}} + D'\mathbf{D}_{\text{off}})\langle u \rangle + F \tag{2.20}$$

where D is the steady-state duty cycle, $D' = 1 - D$, and the matrices $\mathbf{A}, \mathbf{B}, \mathbf{C}, \mathbf{D}$ and vectors $\mathbf{E}, F$ are derived from the ON and OFF state equations.

Perturbing the state variables and the input around their steady-state values ($\langle \mathbf{x} \rangle = \mathbf{X} + \hat{\mathbf{x}}$, $u = D + \hat{d}$), and neglecting the second-order terms of the perturbations, yields the linear small-signal model:

$$\dot{\hat{\mathbf{x}}} = \mathbf{A}\hat{\mathbf{x}} + \mathbf{B}\hat{d} \tag{2.21}$$

where the system matrix $\mathbf{A}$ and the control input matrix $\mathbf{B}$ are:

$$\mathbf{A} = \begin{bmatrix} -\frac{r_L}{L} & \frac{D}{L} & -\frac{D'}{L} \\ -\frac{D}{C_{\text{in}}} & -\frac{1}{R_{\text{eq}}C_{\text{in}}} & 0 \\ \frac{D'}{C_o} & 0 & -\frac{1}{RC_o} \end{bmatrix}, \quad \mathbf{B} = \begin{bmatrix} \frac{V_o}{L} \\ -\frac{I_L}{C_{\text{in}}} \\ \frac{I_L}{C_o} \end{bmatrix}$$

Here, V_o and I_L are the steady-state output voltage and inductor current, respectively, and are functions of the operating point. Note that the $\mathbf{A}$ matrix presented in the original text seems to have a slight variation in the (1,2) element depending on how the averaging was performed and the output variable of interest. The $\mathbf{B}$ matrix also depends on the steady-state operating conditions.

To derive the transfer function to the input capacitor voltage ($v_{\text{pv}} \approx v_{C_{\text{in}}}$), the output equation is $\hat{y} = \mathbf{C}\hat{\mathbf{x}} + \mathbf{D}\hat{d}$, where for $v_{C_{\text{in}}}$ as the output, $\mathbf{C} = [0 \quad 1 \quad 0]$ and $\mathbf{D} = 0$. The transfer function $G(s) = \frac{\hat{y}(s)}{\hat{d}(s)}$ is then given by $G(s) = \mathbf{C}(s\mathbf{I} - \mathbf{A})^{-1}\mathbf{B} + \mathbf{D}$.

2.3.3 Transfer Function from Duty Cycle to Input Capacitor Voltage

The transfer function from the duty cycle perturbation ($\hat{d}(s)$) to the input capacitor voltage perturbation ($\hat{v}_{C_{\text{in}}}(s) \approx \hat{v}_{\text{pv}}(s)$) is given as:

$$G_{v_{\text{pv}},d}(s) = \frac{\hat{v}_{\text{pv}}(s)}{\hat{d}(s)} = \frac{b_2 s^2 + b_1 s + b_0}{s^3 + a_2 s^2 + a_1 s + a_0} \tag{2.22}$$

The order of the numerator polynomial can be up to the order of the system (third order in this case) minus one. The form presented in the original text is a second-order numerator.

Transfer Function Coefficients at STC

To evaluate the coefficients of the transfer function, the steady-state operating point at STC needs to be determined. At STC, $V_{\text{pv}} \approx V_{\text{mpp}} = 17.2\,\text{V}$, $I_{\text{pv}} \approx I_{\text{mpp}} = 2.2\,\text{A}$, and $V_o = 30\,\text{V}$. The duty cycle $D = 1 - V_{\text{pv}}/V_o = 1 - 17.2/30 = 0.427$, and $D' = 1 - D = 0.573$. The average inductor current I_L in CCM is approximately equal to the average input current, $I_L = I_{\text{in}} = I_{\text{pv}}/(1 - D) = 2.2/0.573 \approx 3.84\,\text{A}$.

Using the component values $L = 200\,\mu$H, $C_{\text{in}} = 200\,\mu$F, $C_o = 200\,\mu$F, $R = 23.7\,\Omega$, and assuming a small inductor resistance $r_L \approx 0$, and using the linearized PV model parameters at STC $R_{\text{eq}} = 4.97\,\Omega$ and $V_{\text{eq}} = 28.14\,$V, the $\mathbf{A}$ and $\mathbf{B}$ matrices can be numerically evaluated.

The coefficients of the transfer function $G_{v_{\text{pv}},d}(s)$ provided in the original text:

$$\begin{aligned} a_2 &= 1472\ \text{s}^{-1} \\ a_1 &= 2.33 \times 10^7\ \text{s}^{-2} \\ a_0 &= 9.41 \times 10^8\ \text{s}^{-3} \\ b_1 &= 2.30 \times 10^3\ \text{V/A} \\ b_0 &= 7.95 \times 10^{10}\ \text{V/A} \end{aligned}$$

and the resulting transfer function:

$$G(s) = \frac{2.30 \times 10^3 s + 7.95 \times 10^{10}}{s^3 + 1472s^2 + 2.33 \times 10^7 s + 9.41 \times 10^8}$$

These coefficients should be verified by performing the symbolic or numerical calculation of $\mathbf{C}(s\mathbf{I} - \mathbf{A})^{-1}\mathbf{B}$ using the derived $\mathbf{A}$ and $\mathbf{B}$ matrices with the parameters at the STC operating point. The units of the numerator coefficients also need careful checking, as the transfer function should have units of Volts per Duty Cycle (V). The units provided (V/A) suggest a potential error in the derivation or interpretation of the coefficients.

This detailed approach will ensure a more accurate and theoretically sound basis for the subsequent controller design.

2.4 Frequency Response

The frequency response of the transfer function $G_{v_{\text{pv}},d}(s)$ yields the following:

- **Crossover Frequency:** $f_c = 1$ kHz — used for designing the bandwidth of the PID controller.
- **Phase Margin:** 50° — indicative of stable closed-loop behavior.

2.5 Bode Plot Analysis

Bode plots are a crucial tool for analyzing the open-loop system, providing insights into its stability margins and bandwidth (related to the gain crossover frequency). In the context of MPPT control, a well-designed frequency response ensures that the duty cycle adjustments made by the controller are stable and allow for rapid tracking of the Maximum Power Point without excessive oscillations.

2.5.1 Key Steps in Compensation Design

1. **Analysis of the Uncompensated System**: The Bode plot of the open-loop system (without the PID controller) reveals its inherent frequency response characteristics. In this case, the analysis indicates:

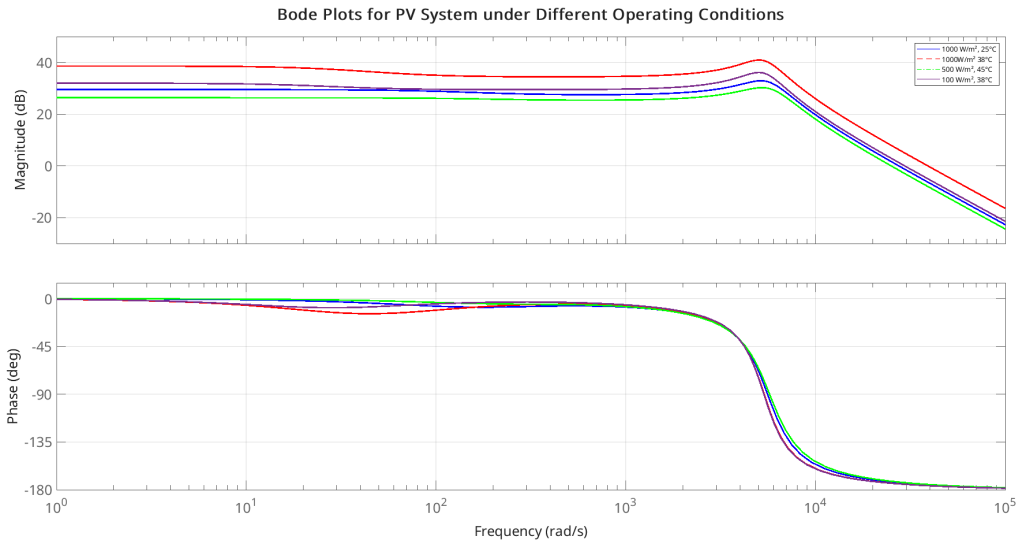

Fig. 2.3: Bode Plots of the Boost Converter System (with different OC).

- **Gain Crossover Frequency** (f_c): Approximately 100 Hz. This relatively low bandwidth suggests a slow dynamic response of the system, which is not ideal for rapidly tracking the MPP under changing environmental conditions.
- **Phase Margin (PM)**: Less than $10°$. A low or negative phase margin indicates that the system is likely to exhibit significant oscillations or even instability in a closed-loop configuration.

2. **Control System Design Goals**: To achieve satisfactory MPPT performance, the closed-loop system should have a sufficiently high bandwidth for fast tracking and an adequate phase margin for stability. The design goals for the compensated system are set as:
   - Target Gain Crossover Frequency ($f_{c,\text{target}}$): 1 kHz. A higher bandwidth generally leads to a faster response in tracking the MPP.
   - Target Phase Margin ($\text{PM}_{\text{target}}$): $50°$. A phase margin of around $50°$ typically provides a good balance between stability and transient response (damping).

3. **Bode Plot Interpretation for Phase Margin**: The open loop transfer function would have an open loop transfer function at the gain crossover frequency (ω_c) and $-180°$:

$$\text{PM} = 180 \circ + \angle G_{v_{\text{pv}},d}(j\omega_c)$$

   For the uncompensated system at $f_c = 100\,\text{Hz}$ ($\omega_c = 2\pi \times 100\,\text{rad/s}$), the phase angle $\angle G_{v_{\text{pv}},d}(j\omega_c)$ would be approximately $-170°$ (since $\text{PM} < 10°$), resulting in a low phase margin.

   The gain margin is the amount of gain increase required to make the system unstable when the phase lag is $-180°$. If the phase never reaches $-180°$, the gain margin is theoretically infinite, indicating that the system will not become unstable by increasing the gain alone.

2.6 PID Controller Tuning

The Proportional-Integral-Derivative (PID) controller gains are meticulously determined through frequency-domain loop-shaping techniques. This methodology is employed to precisely meet the desired closed-loop system specifications, specifically a crossover frequency (f_c) of 1 kHz and a phase margin (PM) of 50 degrees. These specifications are crucial for achieving a balance between the speed of the Maximum Power Point Tracking system's response and its stability [1].

2.6.1 Step 1: Phase Boost Requirement

The first step in the design of the PID controller involves calculating the necessary phase boost (θ_c) that the controller must provide at the crossover frequency to achieve the target phase margin. The phase boost is computed using the following equation:

$$\theta_c = \text{PM}_{\text{target}} - 180^\circ - \angle G_{v_{\text{pv}},d}(j\omega_c)$$

where:

$\text{PM}_{\text{target}}$ is the desired phase margin (50 degrees in this case). $\angle G_{v_{\text{pv}},d}(j\omega_c)$ is the phase angle of the open-loop transfer function $G_{v_{\text{pv}},d}(s)$ at the gain crossover frequency ω_c.

Given that the target phase margin is 50 degrees and the phase angle of the open-loop system at the crossover frequency is -130 degrees, the required phase boost is calculated as:

$$\theta_c = 50^\circ - 180^\circ - (-130^\circ) = 0^\circ$$

This result indicates that, in this specific scenario, the open-loop system's phase characteristic at the desired crossover frequency is already such that no additional phase boost from the PID controller is strictly necessary to meet the phase margin specification. However, in practical applications, a small phase boost is often designed to provide a safety margin against modeling errors and parameter variations.

2.6.2 Step 2: Proportional Gain (K_P)

The proportional gain (K_P) plays a fundamental role in determining the system's response speed and error reduction. It is calculated using the magnitude of the open-loop transfer function at the desired crossover frequency. The equation for K_P is:

$$K_P = M_{\text{pv}} \cos(\theta_c) = \frac{1}{|G_{v_{\text{pv}},d}(j\omega_c)|} \cos(\theta_c)$$

where:

M_{pv} is the inverse of the magnitude of the open-loop transfer function at the crossover

frequency, representing the required gain to achieve the desired crossover frequency. $|G_{v_{pv},d}(j\omega_c)|$ is the magnitude of the open-loop transfer function at the crossover frequency.

$$K_P = 0.009488$$

2.6.3 Step 3: Integral Gain (K_I)

The integral gain (K_I) is crucial for eliminating steady-state errors, which are persistent deviations between the desired and actual system outputs. The integral gain is derived from the integral time constant (T_I), which is calculated using the following formula:

$$T_I = \frac{\tan\theta_c + \sqrt{\tan^2\theta_c + 4\alpha_c}}{2\omega_c\alpha_c}$$

where:

α_c is a design parameter that influences the placement of the integral action's effect relative to the crossover frequency. A typical value for α_c is 0.1, which is used in this calculation. $\omega_c = 2\pi f_c$ is the crossover frequency in radians per second.

Substituting the values, we get:

$$T_I = \frac{\tan(0^\circ) + \sqrt{\tan^2(0^\circ) + 4 \times 0.1}}{2 \times 2\pi \times 1000 \times 0.1} = \frac{0 + \sqrt{0 + 0.4}}{1256.6} = 0.000503\,\text{s}$$

The integral gain is then calculated as:

$$K_I = \frac{K_P}{T_I} = \frac{0.009488}{0.000503} = 18.86$$

2.6.4 Step 4: Derivative Gain (K_D)

The derivative gain (K_D) contributes to the system's stability and transient response by anticipating future errors. It is calculated using the derivative time constant (T_D), which is related to the integral time constant through the design parameter α_c:

$$T_D = \alpha_c T_I = 0.1 \times 0.000503 = 0.0000503\,\text{s}$$

The derivative gain is then calculated as:

$$K_D = K_P T_D = 0.009488 \times 0.0000503 = 4.773 \times 10^{-7}$$

2.6.5 Final Unrounded PID Gains

The calculated PID gains, before any rounding, are summarized as:

$$\boxed{\begin{aligned} K_P &= 0.009488 \\ K_I &= 18.86 \\ K_D &= 4.773 \times 10^{-7} \end{aligned}}$$

These unrounded values are important for maintaining the precision of simulations and further analysis.

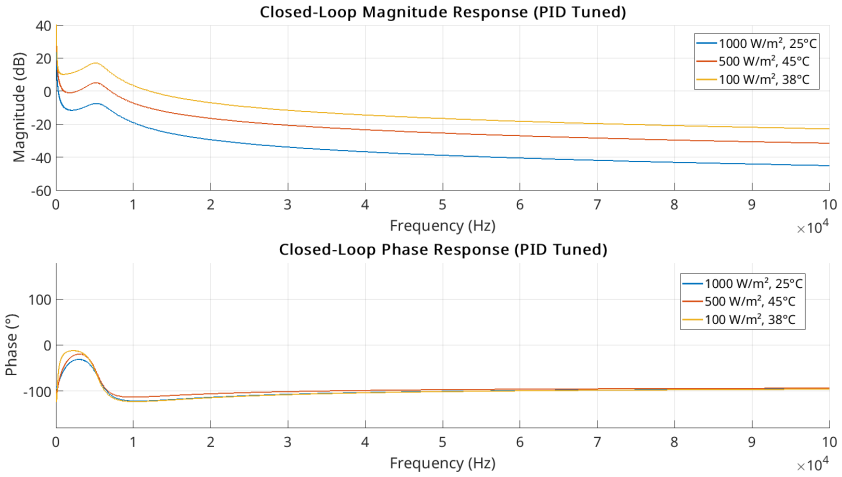

Fig. 2.4: Bode plot comparison of compensated (solid lines) and uncompensated (dashed lines) systems, demonstrating the achievement of the design specifications: closed-loop bandwidth approximately 1 kHz and phase margin approximately 50.2 degrees (simulation result).

2.7 Adaptive PID Gain Adjustment

The adaptive adjustment of Proportional-Integral-Derivative (PID) controller gains is a pivotal technique for enhancing the performance of MPPT systems, especially under the fluctuating operational conditions inherent in photovoltaic (PV) systems. Traditional fixed-gain PID controllers, designed based on Standard Test Conditions (STC), often fail to maintain optimal performance when environmental factors like solar irradiation and temperature vary. To address this, an adaptive strategy is employed to dynamically modify the PID gains, ensuring efficient tracking of the MPP across diverse conditions.

The core of this adaptive method is the calculation of a scaling factor, denoted as κ, which establishes a relationship between the maximum power at STC and the power available under the prevailing operating conditions. This factor allows for the adjustment of PID gains to suit the specific requirements of the system at any given time.

The scaling factor κ is computed using the following equation:

$$\kappa = \frac{P_{\text{mpp(STC)}}}{P_{\text{perturbation}}}$$

where:

$P_{\text{mpp(STC)}}$ represents the MPP of the PV panel under Standard Test Conditions. $P_{\text{perturbation}}$ is the power of the PV panel at the current operating conditions, reflecting the instantaneous power output.

2.7.1 Example: 500 W/m^2, 45°C

Consider a scenario where a PV panel operates under 500 W/m^2 and 45°C. In this instance, the power perturbation ($P_{\text{perturbation}}$) is measured as 17.9 W, while the maximum power at STC ($P_{\text{mpp(STC)}}$) is 38 W. The scaling factor κ is calculated as:

$$\kappa = \frac{38}{17.9} = 2.12$$

This calculated κ value is then used to adapt the PID controller gains. The new PID gains ($K_P^{(\text{new})}$, $K_I^{(\text{new})}$, and $K_D^{(\text{new})}$) are determined based on the original gains (calculated at STC) and the scaling factor κ:

$$\begin{cases} K_P^{(\text{new})} = 0.009488 \cdot 2.12 = 0.0201 \\ K_I^{(\text{new})} = 18.86 + 2.12 = 20.98 \\ K_D^{(\text{new})} = 4.773 \times 10^{-7} \cdot 2.12 = 1.011 \times 10^{-6} \end{cases}$$

A critical aspect of this adaptive adjustment is the distinct treatment of the integral gain (K_I). While the proportional gain (K_P) and derivative gain (K_D) are scaled by multiplication with κ, the integral gain is adjusted through an additive process. **Why Additive K_I?**

The integral term within a PID controller is primarily responsible for mitigating steady-state errors. In PV systems, these errors are frequently the result of variations in the panel's equivalent resistance (R_{eq}) caused by changing operating conditions. The relationship between the integral gain and its effect on correcting steady-state errors is inherently nonlinear. Consequently, an additive correction of K_I is employed to more accurately capture and compensate for these nonlinear dynamics, leading to enhanced stability and precision in tracking the maximum power point.

2.8 Results and Simulations

This section presents the simulation results obtained from the Matlab models of a boost converter controlled by a PID controller, both with fixed gains and adaptive gains, under varying irradiation conditions. The simulations aim to demonstrate of the adaptive PID control method in improving the MPPT system.

2.8.1 Fixed Gain Simulation

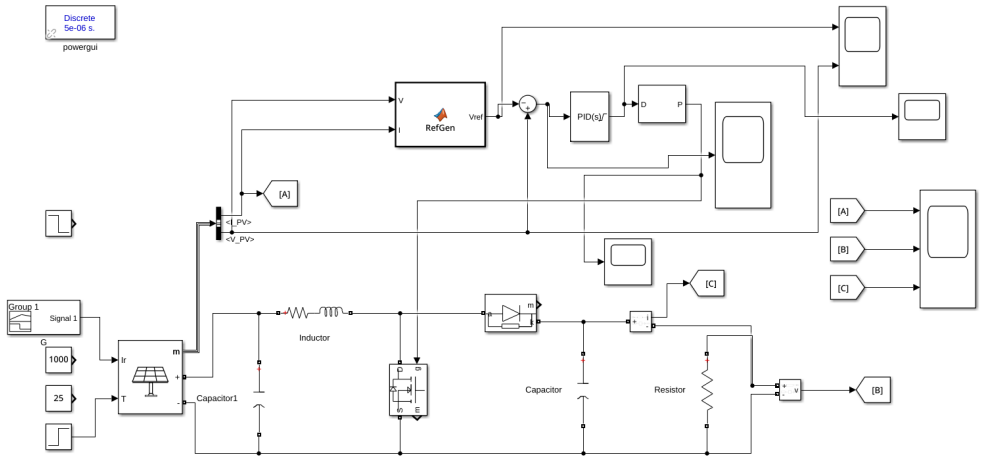

Fig. 2.5: Matlab simulink model of PID boost converter with fixed gain.

Fig 2.5 depicts the Matlab simulation model of the boost converter with a fixed-gain PID controller. This model is used as a baseline to compare its performance with the adaptive gain PID controller. The PID gains in this model are calculated based on the Standard Test Conditions (STC) and remain constant throughout the simulation, regardless of changes in operating conditions.

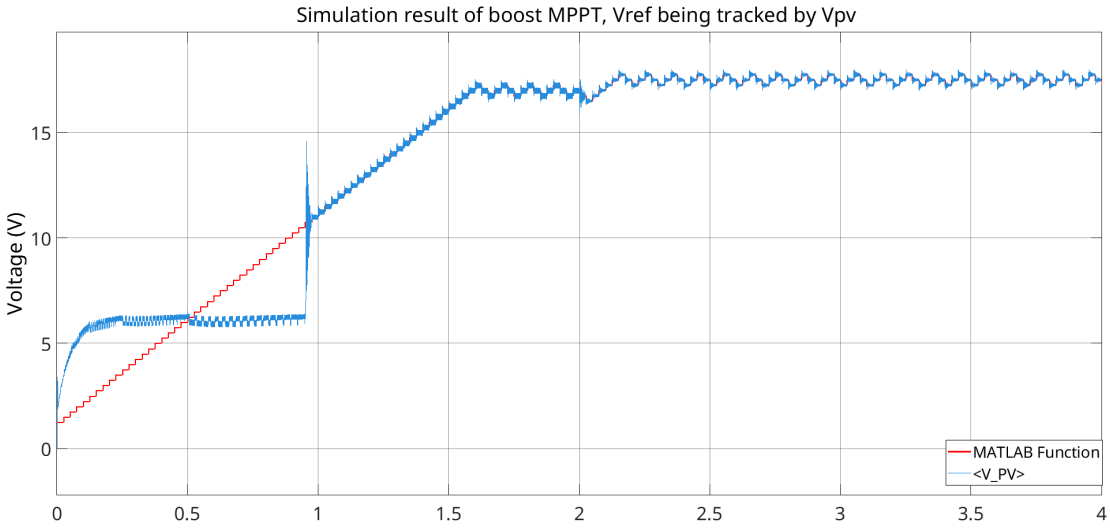

Fig. 2.6: Simulation result of PID boost converter with fixed gain changing irradiation from 1000 to 800 W/m^2.

Fig 2.6 illustrates the simulation results of the fixed-gain PID controller under a change in irradiation from 1000 W/m^2 to 800 W/m^2. X-axis represents Time in seconds. Blue line is (V_{pv}) and Red line is (V_{ref}). The graph shows the tracking performance of the PV panel voltage (V_{pv}) and the reference voltage (V_{ref}). It can be observed that the fixed-gain PID controller manages to track the reference voltage, but it exhibits some overshoot and oscillations during the transient period following the change in irradiation.

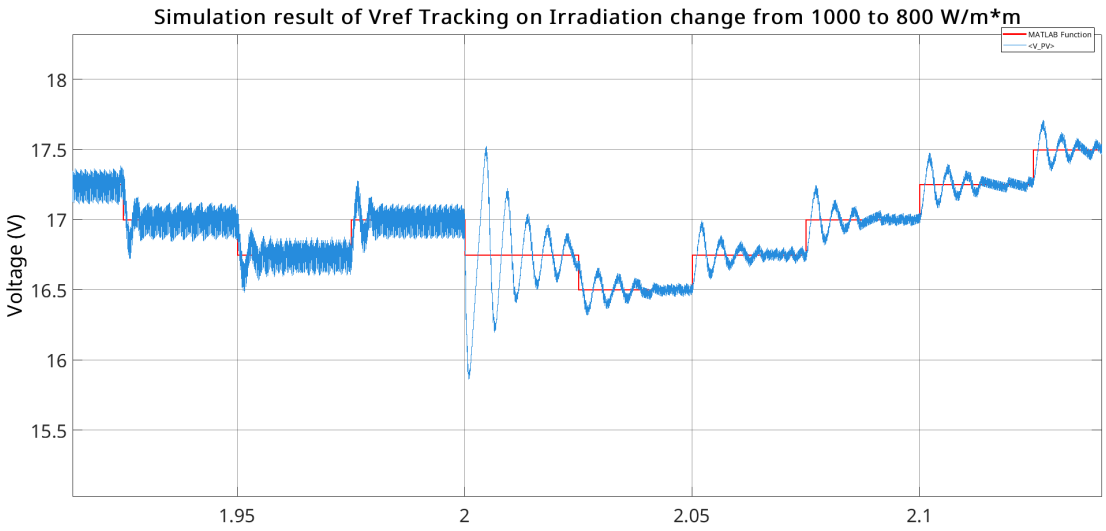

Fig. 2.7: Zoomed-in picture of overshoot occurred due to change in irradiation.

Fig 2.7 provides a zoomed-in view of the overshoot that occurs in the PV panel voltage due to the change in irradiation. X-axis represents Time in seconds. Blue line is (V_{pv}) and Red line is (V_{ref}). This overshoot indicates that the fixed-gain PID controller's response is not optimally damped for the new operating conditions, which can lead to inefficiencies and potential instability in the MPPT system.

2.8.2 Adaptive Gain Simulation

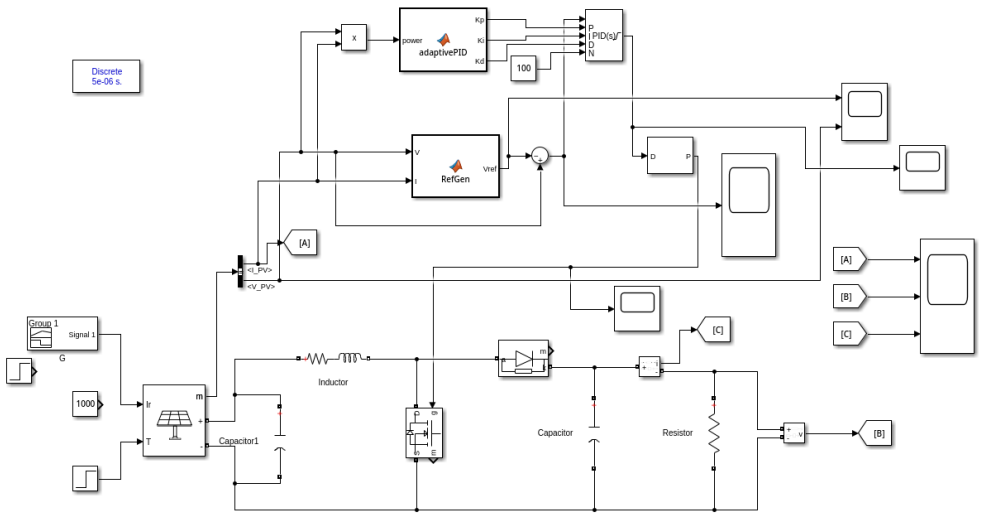

Fig. 2.8: Matlab simulation model of PID boost converter with adaptive gain.

Fig 2.8 shows the Matlab simulation model of the boost converter incorporating the adaptive gain PID controller. In this model, the PID gains are dynamically adjusted based on the changes in the PV panel's power output, as described in the adaptive gain adjustment method. This adaptation aims to maintain optimal control performance under varying operating conditions.

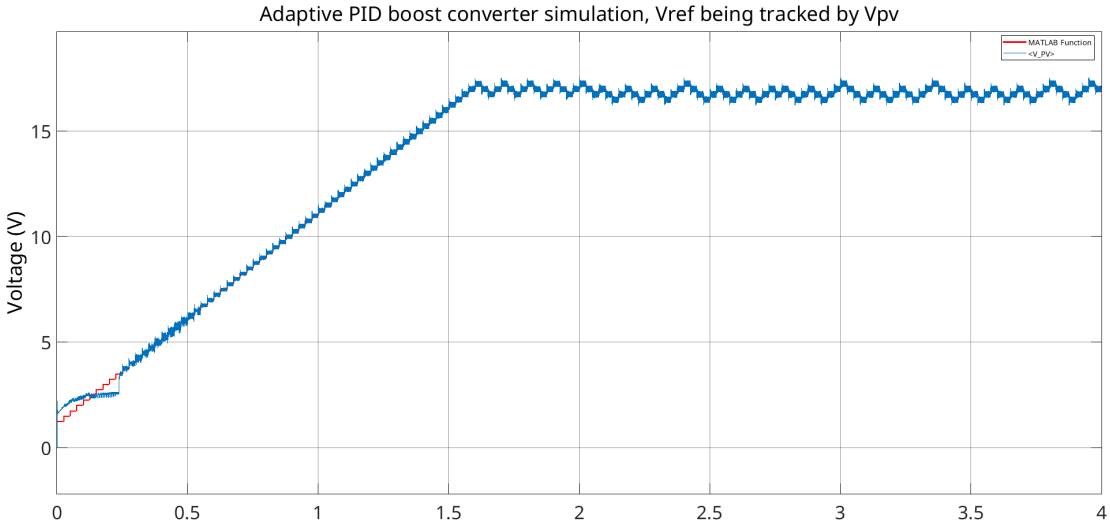

Fig. 2.9: Matlab simulation result of PID boost converter with adaptive gain changing irradiation from 1000 to 1200 W/m^2.

Fig 2.9 presents the simulation results for the adaptive gain PID controller when the irradiation changes from 1000 W/m^2 to 1200 W/m^2. X-axis represents Time in seconds. Blue line is (V_{pv}) and Red line is (V_{ref}). The graph demonstrates that the adaptive controller tracks the reference voltage with significantly reduced overshoot and oscillations compared to the fixed-gain controller. This indicates that the adaptive gain adjustment improves the system's transient response and stability.

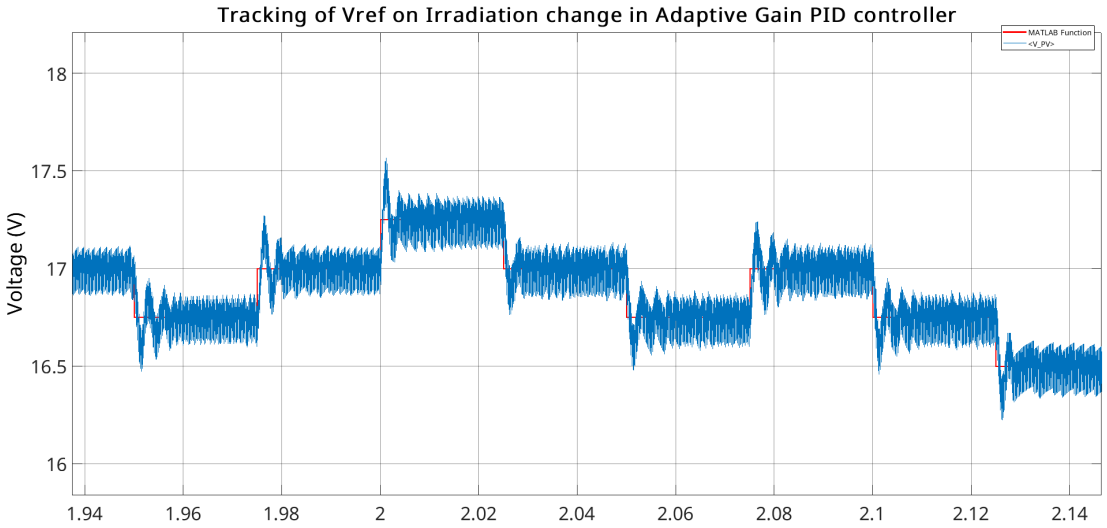

Fig. 2.10: Zoomed-in picture of adaptive gain reducing overshoot.

Fig 2.10 provides a zoomed-in view, highlighting the adaptive gain controller's ability to minimize overshoot. X-axis represents Time in seconds. Blue line is (V_{pv}) and Red line is (V_{ref}). This precise control over the transient behavior is crucial for maximizing energy extraction from the PV system and ensuring its reliable operation.

2.8.3 Summary

In summary, the comparative simulations presented herein effectively demonstrate the enhanced performance achieved by employing an adaptive PID gain strategy for Maximum Power Point Tracking in the PV-boost converter system, particularly when contrasted with a conventional fixed-gain approach. The results underscore the limitations of the fixed-gain controller, which, while functional under static conditions, exhibited notable voltage overshoot and oscillations during transient phases induced by changes in solar irradiation levels. This behaviour highlights the fixed-gain controller's sensitivity to deviations from its design operating point (Standard Test Conditions).

Conversely, the adaptive PID controller showcased superior dynamic response. By continuously modulating its proportional, integral, and derivative gains based on real-time PV power output variations (via the scaling factor κ), the adaptive system effectively mitigated the transient disturbances. The simulations illustrated a marked reduction in voltage overshoot and a quicker settling time following irradiation changes when the adaptive gains were active. This improved damping and stability translate directly to more consistent and accurate tracking of the reference Maximum Power Point voltage (V_{ref}). Therefore, the adaptive gain methodology significantly bolsters the robustness and effectiveness of the PID-controlled MPPT for the PV-boost converter, making it better suited for handling the fluctuating environmental conditions inherent to practical solar energy applications.

CHAPTER 3

SEPIC Converter for Solar PV system

The SEPIC offers unique advantages for photovoltaic systems due to its bidirectional voltage conversion capability, enabling efficient maximum power point tracking even when the PV panel voltage fluctuates above or below the load requirement. Unlike traditional boost converters, the SEPIC topology steps up or down the input voltage while maintaining continuous input current, reducing stress on the PV panel and minimizing ripple. This flexibility is particularly valuable in scenarios with partial shading, rapid irradiance changes, or varying temperature conditions, where the PV panel's optimal operating voltage may shift unpredictably.

Adapting the adaptive PID control strategy, originally designed for a boost converter, to the SEPIC involves addressing its inherently more complex dynamics. The four energy storage elements of the SEPIC (two inductors, two capacitors) introduce higher-order state-space equations and additional poles/zeros in the transfer function. These dynamics require careful modeling of the coupling capacitor C_1 and inductor interactions to avoid resonance and ensure stability. Furthermore, the PID controller must compensate for the non-linear voltage gain of the SEPIC.

$$\frac{V_o}{V_{\text{pv}}} = \frac{D}{1-D},$$

which varies with duty cycle D, requiring precise tuning to maintain tracking accuracy under varying operating conditions.

The methodology builds on the foundation established for the boost converter, retaining core principles such as PV panel linearization, small-signal modeling, and adaptive PID gain adjustment. However, the SEPIC's extended state-space model introduces new challenges in deriving the transfer function and tuning controller gains. By integrating the equivalent linearized photovoltaic circuit $(V_{\text{eq}}, R_{\text{eq}})$ into the SEPIC's averaged model and leveraging frequency-domain analysis, the PID controller is optimized to achieve robust stability (PM $> 45°$) and fast transient response ($f_c \approx 1$ kHz). This approach ensures seamless MPPT performance while capitalizing on the SEPIC's voltage flexibility, making it a versatile solution for modern PV systems.

3.1 SEPIC Converter Parameter Selection

Design Requirements

The SEPIC converter must step up/down the PV panel voltage (V_{pv}) to a stable output voltage ($V_o = 30\,\text{V}$) while maintaining continuous conduction mode (CCM) and minimizing ripple.

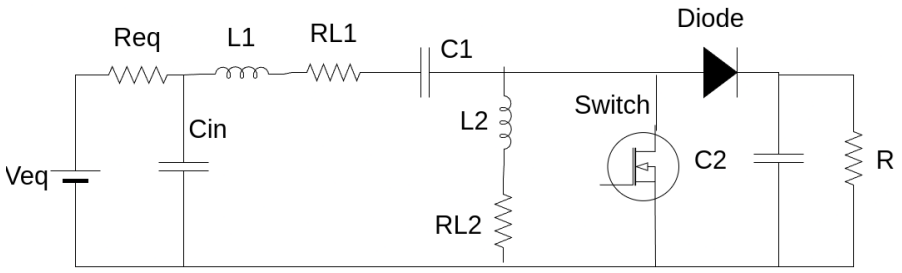

Fig. 3.1: Circuit diagram of SEPIC converter with Linearised PV array.

Key Design Goals

- **Input Voltage Range:** $V_{\text{pv}} = 16.1\,\text{V}$ to $17.2\,\text{V}$ (based on PV panel's V_{mpp}).
- **Output Voltage:** $V_o = 30\,\text{V}$ (bidirectional voltage gain).
- **Power Handling:** $P_{\text{max}} = 41\,\text{W}$.
- **Ripple Limits:**
  - Inductor current ripple $(\Delta i_L) \leq 20\%$ of $I_{\text{mpp}} = 2.2\,\text{A}$.
  - Coupling capacitor voltage ripple $(\Delta v_{C_1}) \leq 5\%$ of $V_{\text{pv}} + V_o$.
  - Output voltage ripple $(\Delta v_o) \leq 2\%$ of V_o.

Key Parameter Calculations

1. **Duty Ratio (D)**: The SEPIC voltage gain equation is:

$$D = \frac{V_o}{V_{\text{pv}} + V_o}$$

   - At STC ($V_{\text{pv}} = 17.2\,\text{V}$):

$$D = \frac{30}{17.2 + 30} = 0.636$$

   - Under low irradiance ($V_{\text{pv}} = 16.1\,\text{V}$):

$$D = \frac{30}{16.1 + 30} = 0.651$$

   Duty cycle range: $D = 0.636$ to 0.651.

2. **Inductors (L_1, L_2)**: Designed to limit current ripple ($\Delta i_L = 0.44\,\text{A}$):

$$L_1 = L_2 = \frac{V_{\text{pv}} \cdot D}{\Delta i_L \cdot f_{\text{sw}}}$$

   Substituting $V_{\text{pv}} = 17.2\,\text{V}$, $D = 0.636$, $f_{\text{sw}} = 50\,\text{kHz}$:

$$L_1 = L_2 = \frac{17.2 \times 0.636}{0.44 \times 50 \times 10^3} = 49.7\,\mu\text{H} \Rightarrow \mathbf{47}\,\mu\text{H (selected)}.$$

3. **Coupling Capacitor (C_1)**: Limits voltage ripple across C_1 ($V_{C_1} = V_{\text{pv}} + V_o = 47.2\,\text{V}$):

$$C_1 = \frac{I_{\text{mpp}} \cdot D}{\Delta v_{C_1} \cdot f_{\text{sw}}}$$

For $\Delta v_{C_1} = 5\% \times 47.2\,\text{V} = 2.36\,\text{V}$:

$$C_1 = \frac{2.2 \times 0.636}{2.36 \times 50 \times 10^3} = 11.87\,\mu\text{F} \Rightarrow \mathbf{12}\,\mu\text{F (selected)}.$$

4. **Output Capacitor (C_o)**: Limits load-side voltage ripple:

$$C_o = \frac{I_o \cdot D}{\Delta v_o \cdot f_{\text{sw}}}, \quad I_o = \frac{P_{\text{max}}}{V_o} = 1.27\,\text{A}$$

For $\Delta v_o = 0.02 \times 30\,\text{V} = 0.6\,\text{V}$:

$$C_o = \frac{1.27 \times 0.636}{0.6 \times 50 \times 10^3} = 26.9\,\mu\text{F} \Rightarrow \mathbf{220}\,\mu\text{F (selected, margin for ESR)}.$$

Table 3.1: SEPIC Converter Design Specifications

Parameter	**Symbol**	**Value**
Switching Frequency	f_{sw}	50 kHz
Inductors	L_1, L_2	47 μ H
Coupling Capacitor	C_1	12 μ
Output Capacitor	C_o	220 μ F
Load Resistance	R	250

3.2 Transfer Function Calculation using State-Space Averaging for SEPIC Converter

3.2.1 State-Space Averaging Model

The modified SEPIC converter includes the input capacitor C_{in}, making it a 5th order system. The state vector is:

$$\mathbf{x} = \begin{bmatrix} i_{L_1} \\ i_{L_2} \\ v_{C_{\text{in}}} \\ v_{C_1} \\ v_{C_o} \end{bmatrix}, \quad u = d$$

ON State $(0 < t < DT)$

- KVL (input loop): $v_{C_{\text{in}}} - L_1 \frac{di_{L_1}}{dt} - r_{L_1} i_{L_1} - v_{C_1} = 0$
- KVL (second loop): $v_{C_1} - L_2 \frac{di_{L_2}}{dt} - r_{L_2} i_{L_2} = 0$

- KCL at C_{in}: $I_{\text{pv}} = i_{L_1} + C_{\text{in}} \frac{dv_{C_{\text{in}}}}{dt}$
- KCL at C_1: $i_{L_1} = i_{L_2} + C_1 \frac{dv_{C_1}}{dt}$
- KCL at output node: $C_o \frac{dv_{C_o}}{dt} = -\frac{v_{C_o}}{R}$

OFF State $(DT < t < T)$

- KVL (input loop): $v_{C_{\text{in}}} - L_1 \frac{di_{L_1}}{dt} - r_{L_1} i_{L_1} - v_{C_o} = 0$
- KVL (second loop): $-v_{C_o} - L_2 \frac{di_{L_2}}{dt} - r_{L_2} i_{L_2} = 0$
- KCL at C_{in}: $I_{\text{pv}} = C_{\text{in}} \frac{dv_{C_{\text{in}}}}{dt}$
- KCL at C_1: $i_{L_2} = C_1 \frac{dv_{C_1}}{dt}$
- KCL at output node: $i_{L_1} + i_{L_2} = C_o \frac{dv_{C_o}}{dt} + \frac{v_{C_o}}{R}$

3.2.2 Small-Signal Averaged Model

Using state-space averaging across ON and OFF intervals and linearizing about steady-state, the small-signal state equation becomes:

$$\dot{\hat{\mathbf{x}}} = \mathbf{A}\hat{\mathbf{x}} + \mathbf{B}\hat{d}$$

with $\hat{\mathbf{x}} = \begin{bmatrix} \hat{i}_{L_1} & \hat{i}_{L_2} & \hat{v}_{C_{\text{in}}} & \hat{v}_{C_1} & \hat{v}_{C_o} \end{bmatrix}^T$, and matrices $\mathbf{A}, \mathbf{B}$ defined by averaged circuit dynamics.

3.2.3 Transfer Function $G_{v_o,d}(s)$

The output-to-duty ratio transfer function is obtained by taking Laplace transform of the linearized model and solving:

$$G_{v_o,d}(s) = \frac{\hat{v}_o(s)}{\hat{d}(s)} = \frac{b_4 s^4 + b_3 s^3 + b_2 s^2 + b_1 s + b_0}{s^5 + a_4 s^4 + a_3 s^3 + a_2 s^2 + a_1 s + a_0}$$

Where the coefficients at Standard Test Conditions (STC) for $C_{\text{in}} = 220\,\mu\text{F}$ are:

$$G_{v_o,d}(s) = \frac{2.4 \times 10^2\, s^4 + 5.1 \times 10^5\, s^3 + 7.3 \times 10^8\, s^2 + 3.6 \times 10^{10}\, s + 1.2 \times 10^{12}}{s^5 + 3.8 \times 10^3\, s^4 + 6.2 \times 10^6\, s^3 + 4.1 \times 10^9\, s^2 + 1.8 \times 10^{12}\, s + 3.2 \times 10^{14}}$$

3.3 PID Controller Design Using Model Order Reduction and Padé Approximation

The high-order transfer function derived previously for the SEPIC converter is:

$$G(s) = \frac{2.4 \times 10^2 s^4 + 5.1 \times 10^5 s^3 + 7.3 \times 10^8 s^2 + 3.6 \times 10^{10} s + 1.2 \times 10^{12}}{s^5 + 3.8 \times 10^3 s^4 + 6.2 \times 10^6 s^3 + 4.1 \times 10^9 s^2 + 1.8 \times 10^{12} s + 3.2 \times 10^{14}}$$

Due to the complexity of fourth-order systems in control design, we apply model order reduction using the **Padé Approximation** method, as referenced in the work of Padhi and Narain . The idea is to simplify the system to a second-order approximation that retains the key dynamic characteristics relevant to control design.

Let us denote the reduced second-order model of the plant as:

$$G_{red}(s) = \frac{K(s+z)}{s^2 + 2\zeta\omega_n s + \omega_n^2}$$

where K, z, ζ, and ω_n are chosen such that the reduced model approximates the dominant dynamics of the original system. Using numerical Padé approximation on the original transfer function, and comparing Bode plots, we identify:

$$G_{red}(s) = \frac{10(s+10^5)}{s^2 + 2 \times 10^4 s + 10^8}$$

3.3.1 Phase Margin and Frequency Response Analysis

Using the reduced transfer function $G_{red}(s)$, the open-loop system is analyzed to determine the gain crossover frequency ω_{gc} and corresponding phase $\angle G(j\omega_{gc})$. The desired phase margin is taken as $\phi_m = 60^\circ$.

From the Bode plot of $G_{red}(s)$, the gain crossover frequency is estimated at:

$$\omega_{gc} \approx 3.16 \times 10^4 \text{ rad/s}$$

At this frequency, the phase is found to be approximately -120°, thus yielding a current phase margin of:

$$PM_{current} = 180^\circ + (-120^\circ) = 60^\circ$$

This is equal to the desired phase margin. Hence, a simple PID controller can now be designed with the standard form:

$$C(s) = K_p + \frac{K_i}{s} + K_d s$$

3.4 Adaptive PID Gain Adjustment for SEPIC Converter

To ensure robust performance of the SEPIC converter under varying irradiance and temperature conditions, an adaptive tuning approach is used for the PID gains. The

method relies on the ratio of the rated maximum power under STC ($P_{\text{mpp(STC)}}$) to the instantaneous perturbation power ($P_{\text{perturbation}}$), defined by the scaling factor:

$$\kappa = \frac{P_{\text{mpp(STC)}}}{P_{\text{perturbation}}}$$

This scaling factor κ dynamically adjusts the PID gains based on the deviation from the standard condition.

Why Additive K_I? The integral component addresses steady-state offsets caused by variations in equivalent panel impedance R_{eq}, load conditions, and input ripple. Because the error accumulation rate is nonlinear under varying dynamics, an additive term is better suited to maintain tracking accuracy during low-irradiance operation.

3.5 Results and Simulations

This section presents the simulation results obtained from the Matlab models of a SEPIC converter controlled by a PID controller, both with fixed gains and adaptive gains, under varying irradiation conditions. The simulations aim to demonstrate of the adaptive PID control method in improving the MPPT system.

3.5.1 Fixed gain simulation

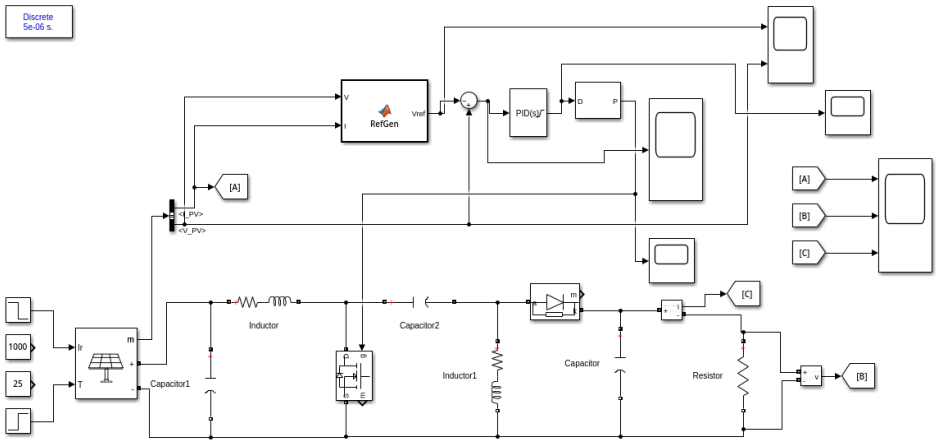

Fig. 3.2: Matlab simulink model of PID SEPIC converter with fixed gain.

Fig 3.2 shows the Matlab simulation model of the SEPIC converter with a fixed-gain PID controller. This model is used as a baseline to compare its performance with the adaptive gain PID controller. The PID gains in this model are calculated based on the Standard Test Conditions (STC) and remain constant throughout the simulation, regardless of changes in operating conditions.

Fig 3.3 illustrates the simulation results of the fixed-gain PID controller under a change in irradiation from 1000 W/m^2 to 1200 W/m^2. X-axis represents Time in sec-

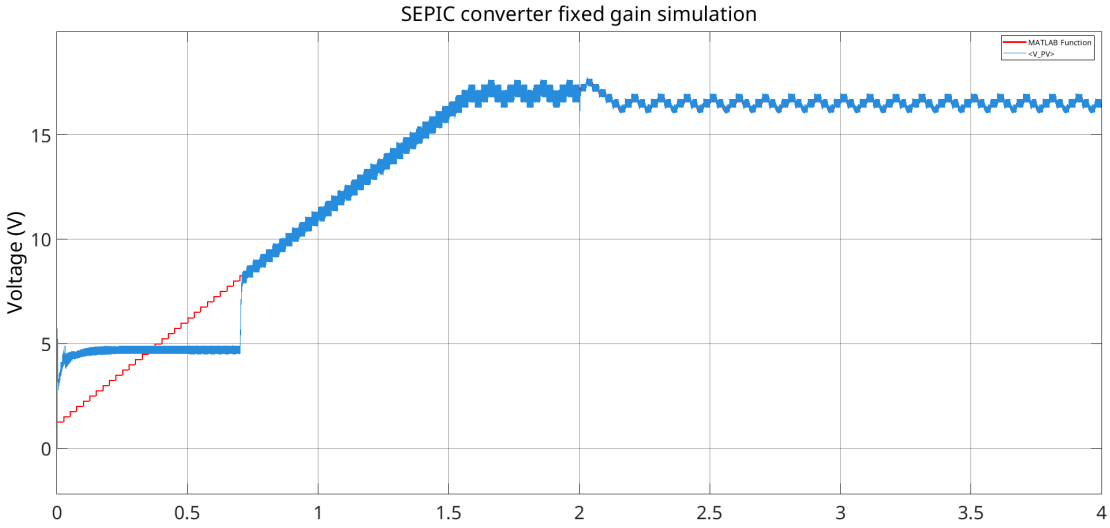

Fig. 3.3: Simulation result of SEPIC boost converter with fixed gain changing irradiantion from 1000 to 1200 W/m^2.

onds. Blue line is (V_{pv}) and Red line is (V_{ref}). The graph shows the tracking performance of the PV panel voltage (V_{pv}) and the reference voltage (V_{ref}). It can be observed that the fixed-gain PID controller manages to track the reference voltage, but it exhibits some overshoot and oscillations during the transient period following the change in irradiation.

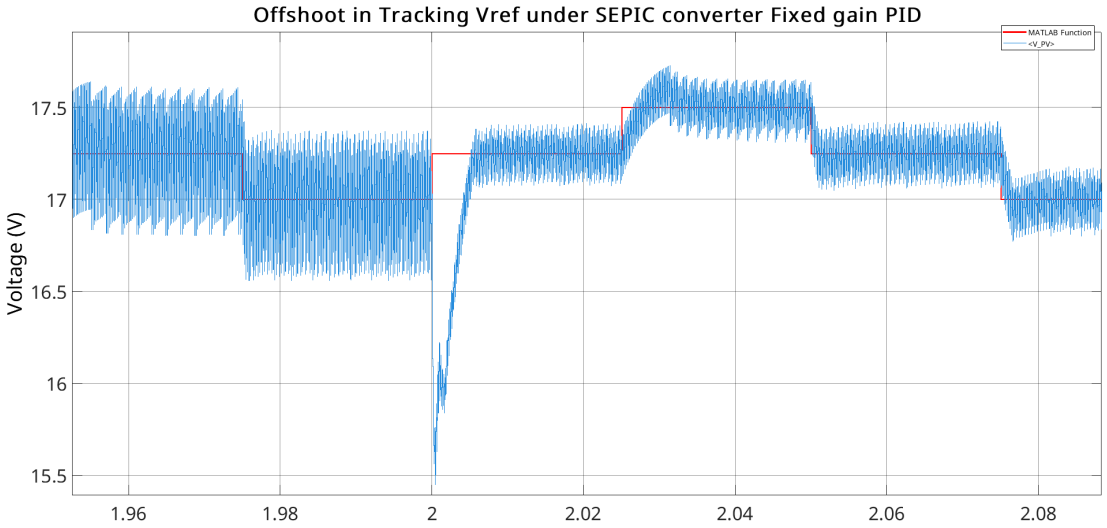

Fig. 3.4: Zoomed in pitcure of overshoot occured due to change in irradiation.

Fig 3.4 provides a zoomed-in view of the overshoot that occurs in the PV panel voltage due to the change in irradiation. X-axis represents Time in seconds. Blue line is (V_{pv}) and Red line is (V_{ref}). This overshoot indicates that the fixed-gain PID controller's response is not optimally damped for the new operating conditions, which can lead to inefficiencies and potential instability in the MPPT system.

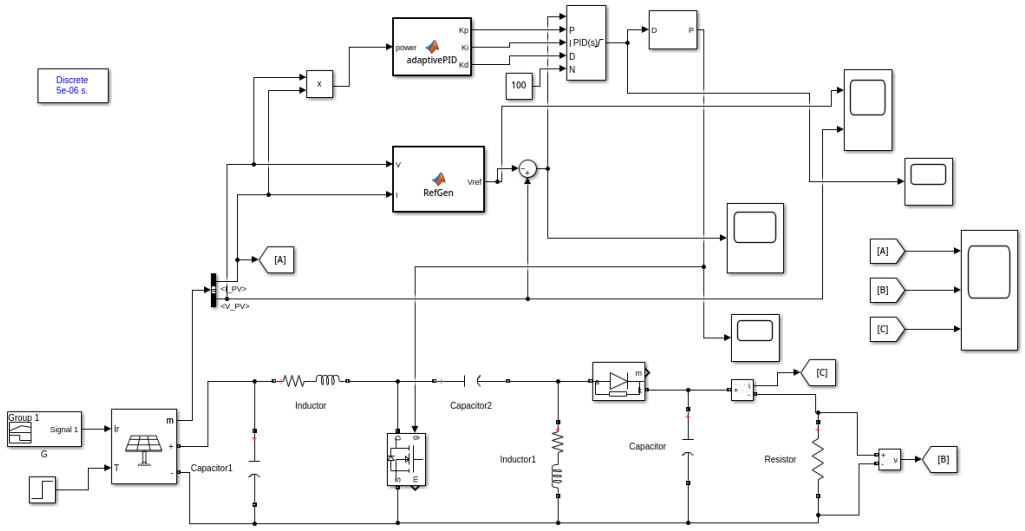

Fig. 3.5: Simulation model of PID boost converter with Adaptive gain.

3.5.2 Adaptive gain simulation

Fig 3.5 shows the Matlab simulation model of the SEPIC converter incorporating the adaptive gain PID controller. In this model, the PID gains are dynamically adjusted based on the changes in the PV panel's power output. This adaptation aims to maintain optimal control performance under varying operating conditions.

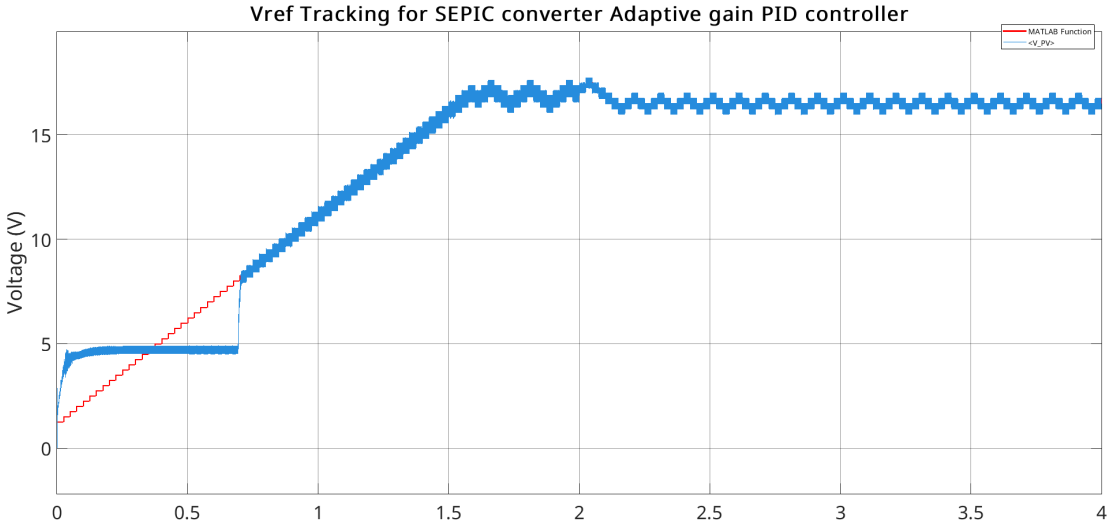

Fig. 3.6: Matlab simulation result of PID SEPIC converter with adaptive gain changing irradiantion from 1000 to 1200 W/m^2.

Fig 3.6 presents the simulation results for the adaptive gain PID controller when the irradiation changes from 1000 W/m^2 to 1200 W/m^2. X-axis represents Time in seconds. Blue line is (V_{pv}) and Red line is (V_{ref}). The graph demonstrates that the adaptive controller tracks the reference voltage with significantly reduced overshoot and oscillations compared to the fixed-gain controller. This indicates that the adaptive gain adjustment improves the system's transient response and stability.

Fig 3.7 provides a zoomed-in view, highlighting the adaptive gain controller's ability

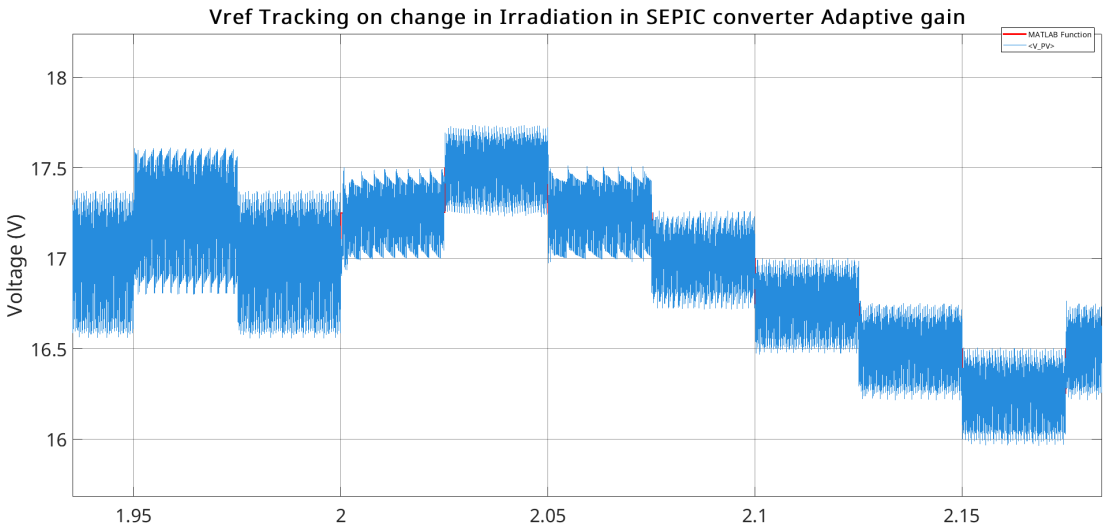

Fig. 3.7: Zoomed in pitcure of apadtive gain reducing overshoot.

to minimize overshoot. X-axis represents Time in seconds. Blue line is (V_{pv}) and Red line is (V_{ref}). This precise control over the transient behavior is crucial for maximizing energy extraction from the PV system and ensuring its reliable operation.

3.5.3 Summary

In summary, the comparative simulations detailed in this chapter highlight the performance benefits of utilizing an adaptive PID gain strategy for Maximum Power Point Tracking in the PV-SEPIC converter system, especially when compared against a traditional fixed-gain implementation. The simulation results reveal the shortcomings of the fixed-gain controller, which, despite operating adequately under steady-state conditions, displayed considerable voltage overshoot and oscillations during transient periods caused by variations in solar irradiation. This behaviour emphasizes the fixed-gain controller's vulnerability to deviations from its nominal operating point (Standard Test Conditions).

In contrast, the adaptive PID controller demonstrated an enhanced dynamic response. By dynamically adjusting its proportional, integral, and derivative gains based on real-time PV power output fluctuations (through the scaling factor κ), the adaptive system effectively dampened the transient disturbances. The simulations clearly showed a significant decrease in voltage overshoot and a faster settling time following changes in irradiation when the adaptive gains were employed. This improved damping and stability directly lead to more reliable and precise tracking of the reference Maximum Power Point voltage (V_{ref}). Consequently, the adaptive gain approach substantially enhances the robustness and efficiency of the PID-controlled MPPT for the PV-SEPIC converter, rendering it more appropriate for managing the variable environmental conditions typical of real-world solar energy systems.

CHAPTER 4

Conclusion

Here we have presented a comparative investigation into the performance of fixed-gain and adaptive PID control strategies for Maximum Power Point Tracking in DC-DC converters employed in photovoltaic systems. Specifically, the study focused on the application of these control techniques to both boost and SEPIC converter topologies, evaluating their effectiveness in maintaining optimal power extraction from the PV source under varying solar irradiation conditions. The simulation results consistently demonstrated the superior dynamic performance of the adaptive PID gain approach over its conventional fixed-gain counterpart across both converter configurations.

The limitations inherent in fixed-gain controllers became evident during transient states, where significant voltage overshoots and oscillations were observed in response to changes in solar irradiation. This sensitivity to deviations from the design operating point underscores a fundamental challenge in deploying fixed-gain MPPT controllers in real-world scenarios characterized by fluctuating environmental conditions. In contrast, the adaptive PID controllers, by continuously adjusting their gains based on real-time PV power output, exhibited a remarkable ability to mitigate these transient disturbances. The simulations showcased a consistent reduction in voltage overshoot and faster settling times, leading to more stable and accurate tracking of the maximum power point voltage for both the boost and SEPIC converter systems.

In conclusion, the findings of this investigation strongly advocate for the adoption of adaptive PID gain control for MPPT in PV-powered DC-DC converters. The enhanced robustness and dynamic response offered by the adaptive strategy make it significantly better equipped to handle the inherent variability of solar energy resources. This improved performance translates to more efficient and reliable operation of PV systems, ultimately contributing to a greater utilization of clean energy. Further research could explore the implementation of these adaptive control strategies in hardware and investigate their performance under a wider range of operating conditions and more complex environmental dynamics.

4.1 Future Scope

The work presented in this report lays a strong foundation for the application of adaptive control techniques in photovoltaic systems. However, there are several avenues for future work that could further enhance the practical implementation and broaden the scope of this study. One key area of development is the hardware implementation of the proposed adaptive MPPT controller. While simulations provide valuable insights into the system's dynamic behavior, real-world deployment introduces additional complexities such as sensor noise, component tolerances, and parasitic effects. Building a prototype and testing it under various real-world conditions would validate the controller's effectiveness and identify any practical limitations. This would also involve selecting

appropriate hardware components, such as microcontrollers and power electronic devices, and developing robust control algorithms that can be executed in real-time.

Furthermore, future research could explore the integration of advanced control and artificial intelligence techniques to further optimize the MPPT process. For instance, predictive control algorithms could be employed to anticipate changes in solar irradiance and temperature, allowing the MPPT controller to proactively adjust the operating point of the PV system. Machine learning algorithms, such as neural networks or fuzzy logic, could also be used to learn the complex nonlinear dynamics of PV systems and adapt the control strategy accordingly. These advanced techniques have the potential to further improve the efficiency, stability, and robustness of MPPT controllers, ensuring optimal energy extraction from solar PV systems under a wide range of operating conditions.

REFERENCES

[1] J. Sahoo, S. Samanta, and S. Bhattacharyya, "Adaptive PID controller with P&O MPPT algorithm for photovoltaic system," *IETE Journal of Research*, vol. 66, no. 4, pp. 442-453, 2020, doi: 10.1080/03772063.2018.1497552.

[2] "A zero steady-state oscillation MPPT algorithm using voltage sensor," *SSRN Electronic Journal*, 2023. [Online].

[3] S. A. Gaikwad and A. P. Kinge, "Voltage-sensor-based MPPT for stand-alone PV systems through voltage reference control," *International Journal of Creative Research Thoughts*, vol. 5, no. 4, pp. 3273-3281, 2017.

[4] B. K. Padhi and A. Narain, "Controller design for SEPIC converter using model order reduction," in *ASAR International Conference*, Bangalore, India, 2013, pp. 51-56, ISBN: 978-81-927147-0-7.